Supplementary Materials

Methods

Data quality control

Four studies included data of two patient groups (Alzheimer I and MCI I, Alzheimer II and MCI II, ADHD and ASD, and ALS and PLS). To minimize inter-group dependencies in the analyses, control subjects were randomly split into two equally sized groups, such that all patient groups had disjoint control groups.

To ensure the quality of all data, outliers among connectivity matrices were identified and subjects were matched in datasets with significant differences in age or gender between patients and controls ($p < 0.05$). Outlier detection was performed on patients and controls of each dataset separately. Automatic outlier detection was used based on the deviation of subjects' connectivity from the group average on three summary measures. The first two measures quantified the presence of odd connections and the absence of common connections. For this, the prevalence of every connection was calculated as the percentage of subjects in which a connection was reported. The first measure computed the average prevalence of all connections present in the reconstructed brain network of a subject, with low average prevalence scores indicating the presence of odd connections. The second measure computed the average prevalence of the connections not present in the reconstructed brain network of the subject, with high values indicating the absence of common connections. The third measure was the average fractional anisotropy of all connections in the reconstructed brain network of a subject. For each of these measures the interquartile range (IQR) was calculated by IQR = Q3 - Q1, with Q3 and Q1 being the 75^{th} and 25^{th} percentiles respectively. Connectivity matrices with a score below Q1-2×IQR or above Q2+2×IQR for

any of the three measures were considered outliers. In total, 62 outliers were detected. Per study the number of outliers ranged between 0 and 9 (SI Table 2). Outliers were excluded from data analysis.

In eight datasets (schizophrenia I, schizophrenia II, bipolar disorder, PTSD II, AD I, MCI I, ALS and PLS), subjects showed significant differences ($\alpha = 0.05$) in age and/or gender. Therefore, in these datasets patient and control groups were matched in the following way: a propensity score was calculated for each subject in a dataset as the probability of a subject being patient predicted by a logistic regression model using age and gender as predictors. The smallest group (either patients or controls) were one-to-one matched with the larger group using nearest neighbor matching of the propensity score (Austin, 2011). After matching, the datasets included 107/107 (schizophrenia I), 23/23 (schizophrenia II), 82/82 (bipolar disorder), 40/40 (PTSD II), 19/19 (AD I), 28/28 (MCI I), 45/45 (ALS), 32/32 (PLS) patients/controls, with no significant differences in age or gender ($\alpha = 0.05$).

MRI acquisition

Patients and controls from the schizophrenia (dataset I and II), bipolar disorder, ADHD, ASD, PTSD (dataset I), ALS and PLS datasets were all scanned with the same image acquisition protocol (an overview of scanner protocols is provided in SI Table 1). Schizophrenia dataset I was previously described in context of fitness therapy and the outcome of psychosis and contributed by W.C. (Svatkova et al., 2015), dataset II was previously described in context of genetic risk and outcome of psychosis and contributed by W.C. and R.S.K. (Collin et al., 2014). Data on bipolar disorder was previously examined in context of altered connectome architecture in bipolar disorder and contributed by N.E.M, M.P.B. and R.A.O. (Collin et al., 2016). The investigated datasets on ASD and ADHD were

previously described in context of developmental differences in children with ASD and ADHD and contributed by S.D. (van Belle et al., 2015). Dataset I on PTSD was previously examined in context of white matter differences in veterans with PTSD and contributed by E.G. (Kennis et al., 2015). Datasets on ALS and PLS were contributed and previously described by L.v.d.B. (van der Burgh et al., 2016; Verstraete et al., 2011; Walhout et al., 2015). Data was acquired for each participant on a 3 Tesla Philips Achieva MRI scanner (Philips Healthcare, Best, the Netherlands). Imaging included the acquisition of a T1-weighted image (parameters: 3D FFE, TE = 4.6ms, 0.75 mm isotropic voxel size) and two DWI sets each consisting of 30 diffusion-weighted volumes (b0-value: 1000 s/mm^2) and five diffusion-unweighted volumes (parameters: SENSE parallel imaging; TE = 68 ms, 2 mm isotropic voxel size, second set with reversed phase-encoding direction).

Data of Alzheimer's disease dataset I and MCI dataset I were previously analyzed and described by M.M. and M.B. (Mancini et al., 2016; Serra et al., 2016). Data was acquired on a 3 Tesla Magnetom Allegra MRI scanner (Siemens, Erlangen, Germany). Data included the acquisition of a T1-weighted image (parameters: 3D MDEFT, TE = 2.4 ms, 1.0 mm isotropic voxel size) and a DWI set including 61 diffusion weighted volumes (b0-value: 1000 s/mm^2) and seven diffusion-unweighted volumes (parameters: TE = 2.4 ms, 2.3 mm isotropic voxel size).

Data of Alzheimer's disease II, MCI II and PTSD II were collected from the Alzheimer's Disease Neuroimaging Initiative (ADNI) database (adni.loni.usc.edu, for further information see www.adni-info.org, (Jack et al., 2008)). The primary goal of ADNI has been to test whether serial magnetic resonance imaging (MRI), positron emission tomography (PET), other biological markers, and clinical and neuropsychological assessment can be combined to measure the progression of mild cognitive impairment (MCI) and early Alzheimer's disease (AD). We selected data from the first visit of each subject in the ADNI

dataset (either ADNIGO screening visit, ADNI2 screening, or ADNI2 Initial Visit). This data was acquired on either a Signa HDxt or Discovery MR 750 3 Tesla MRI scanner (GE Medical Systems, Milwaukee, Wisconsin). MRI scanning consisted of a T1-weighted scan (parameters: Saggital IR-SPGR, TE = 3.0 (Signa HDxt) or 2.8 (Discovery MR 750), 1.0×1.0×1.2 mm voxel size) and a DWI set including with 41 diffusion-weighted volumes (b0-value: 1000 s/mm^2) and five diffusion-unweighted volumes (parameters: TE=minimal, 1.4×1.4×2.7 mm voxel size).

Data of obesity was previously analyzed and described by I.M.I. and M.A.J. (Marqués-Iturria et al., 2015). Data was acquired on a 3 Tesla Siemens Magnetom Trio scanner (Siemens, Erlangen, Germany). Structural imaging included a T1-weighted image (parameters: TE = 2.98 ms, 1.0 mm isotropic resolution) and a DWI set including 30 diffusion-weighted volumes (b0-value: 1000 s/mm^2) and one diffusion unweighted volume (parameters: TE = 89 ms, 2 mm isotropic voxel size).

Data of OCD was previously analyzed and described by T.J.R. and K.K. (Reess et al., 2016). Data was acquired on a 3 Tesla Philips Ingenia MRI scanner (Philips Healthcare, Best, the Netherlands). Structural imaging included a T1-weighted image (parameters: 3D MPRAGE, TE = 4 ms, 1.0 mm isotropic resolution) and a DWI set including 32 diffusion-weighted volumes (b0-value: 1000 s/mm^2) and two diffusion-unweighted volumes (parameters: TE = 57 ms, 2 mm isotropic voxel size).

Data of MDD was previously analyzed and described by J.R., U.D. and S.M. (Repple et al., 2017). Data was acquired on a 3 Tesla Gyroscan Intera MRI scanner (Philips Healthcare, Best, the Netherlands). Structural imaging included a T1-weighted image (parameters: Turbo field echo, TE = 3.4 ms, 0.5 mm isotropic resolution) and a DWI set weighted imaging including 20 diffusion-weighted volumes (b0-value: 1000 s/mm^2) and one diffusion-unweighted volume (parameters: TE = 95 ms, 0.94 ×0.94×3.6 mm voxel size).

Human Connectome Project reference data

A reference human connectome reconstruction was obtained from MRI data of 500 subjects provided in the 500 Subjects release of the Human Connectome Project (Glasser et al., 2013; Van Essen et al., 2012). Structural imaging included a T1-weighted image (0.7 mm isotropic resolution) and a DWI set consisting of 270 diffusion-weighted volumes and 18 diffusion-unweighted volumes (parameters: TE = 89.50 ms, 1.25 mm isotropic resolution). The Human Connectome Project provided preprocessed DWI data that was corrected for motion, eddy current and susceptibility distortions (Glasser et al., 2013). White matter pathways were reconstructed using generalized q-sampling imaging and streamline tractography (Yeh et al., 2010). A HCP group connectome was constructed in which connections were included when they were reported in at least 60% of the subjects (de Reus and van den Heuvel, 2013a). Connections in the HCP group connectome were weighted by the average connectivity strength (fractional anisotropy) reported over all subjects in which a connection was present.

Robustness analyses

Leave-one-out validation

Results were validated by leave-one-out analysis in which cross-disorder involvement maps were recomputed with one disorder left out at a time. Rich club connectivity had in all cases significantly higher cross-disorder involvement levels than reported in local connections (19% – 29% increase, all $p < 0.05$). Rich club connections showed not in all iterations significantly higher cross-disorder involvement compared with feeder connections (12% - 22% increase).

Connections with high betweenness centrality showed significantly increased cross-disorder involvement in all iterations when compared with, also recomputed, cross-disorder involvement maps based on permuted disease effects (19% - 28% increase, all $p < 0.05$). Similarly, significant effects were reported in all iterations for connections with high edge-removal effect on communicability (10% - 17% increase, all $p < 0.05$) and for spatially long connection (44% - 30% increase, all $p < 0.05$).

Desikan-Killiany subparcellation

In the main analysis, connectome maps were reconstructed according to a subparcellation of the Desikan-Killiany atlas with 219 distinct regions (DK-219) (Cammoun et al., 2012; Desikan et al., 2006). Cammoun and colleagues (2012) also presented a coarse subdivision with 114 regions (DK-114, 57 left-hemispheric and 57 right-hemispheric). Topological characteristics of networks have been shown to vary with network size (de Reus and van den Heuvel, 2013b; Zalesky et al., 2010). Therefore, we verified in a post-hoc analysis that using a DK-114 parcellation provided results similar to the results described in the main text that used the DK-219 parcellation.

For all subjects, in the clinical datasets and reference HCP dataset, reconstructed white matter pathways were combined with the individuals' DK-114 parcellation to provide a DK-114 connectome reconstruction. The prevalence threshold of the HCP group connectome map was set to 75%, i.e. connections were included if they were reported in at least 75% of the subjects, to ensure comparable network density between the DK-114 HCP group connectome map (7.95% of the possible connections present) and the DK-219 HCP group connectome map from the main text (7.93% of the possible connections present). Hub regions were selected as regions with regional degree above 12, giving the 14 (12.3%) regions with highest

regional degree (approximating the top 15% regions). Hub regions included parts of the insula, istmus cingulate, paracentral, posterior cingulate, precuneus, superior frontal, superior parietal and superior temporal. This set of hub regions showed a significant rich club organization ($p = 0.0005$, permutation testing with 10,000 degree-preserved rewired networks).

No regions showed significantly higher region-wise cross-disorder involvement than observed in the permuted cross-disorder involvement maps. NBS analysis showed a significantly large subnetwork of connections with cross-disorder involvement above 35% ($p = 0.0002$). This subnetwork included 17 regions and 36 connections, including inferior parietal, paracentral, postcentral, posterior cingulate, precentral, precuneus, superior frontal and superior parietal regions. Rich club connections showed significantly higher cross-disorder involvement levels than reported for local connections (30% increase, $p = 0.0207$). No significant difference in cross-disorder involvement levels were observed between rich club and feeder connections ($p = 0.0859$). Connections with high betweenness scores showed significantly increased cross-disorder involvement when compared with cross-disorder involvement maps based on permuted disease effects (23% increase, $p = 0.0018$). Connections with high edge-removal effect on network communicability showed non-significantly higher cross-disorder involvement than seen in permuted cross-disorder involvement maps (10% increase, $p = 0.0965$). Spatially long connections showed 46% higher cross-disorder involvement compared with cross-disorder involvement levels of permuted maps ($p = 0.0001$).

References

Austin, P. C. (2011). An Introduction to Propensity Score Methods for Reducing the Effects of Confounding in Observational Studies. *Multivariate Behav. Res.* 46, 399–424. doi:10.1080/00273171.2011.568786.

Cammoun, L., Gigandet, X., Meskaldji, D., Thiran, J. P., Sporns, O., Do, K. Q., et al. (2012). Mapping the human connectome at multiple scales with diffusion spectrum MRI. *J. Neurosci. Methods* 203, 386–397. doi:10.1016/j.jneumeth.2011.09.031.

Collin, G., Kahn, R. S., de Reus, M. A., Cahn, W., and van den Heuvel, M. P. (2014). Impaired Rich Club Connectivity in Unaffected Siblings of Schizophrenia Patients. *Schizophr. Bull.* 40, 438–448. doi:10.1093/schbul/sbt162.

Collin, G., van den Heuvel, M. P., Abramovic, L., Vreeker, A., de Reus, M. A., van Haren, N. E. M., et al. (2016). Brain network analysis reveals affected connectome structure in bipolar I disorder. *Hum. Brain Mapp.* 37, 122–134. doi:10.1002/hbm.23017.

de Reus, M. A., and van den Heuvel, M. P. (2013a). Estimating false positives and negatives in brain networks. *Neuroimage* 70, 402–9. doi:10.1016/j.neuroimage.2012.12.066.

de Reus, M. A., and van den Heuvel, M. P. (2013b). The parcellation-based connectome: Limitations and extensions. *Neuroimage* 80, 397–404. doi:10.1016/J.NEUROIMAGE.2013.03.053.

Desikan, R. S., Ségonne, F., Fischl, B., Quinn, B. T., Dickerson, B. C., Blacker, D., et al. (2006). An automated labeling system for subdividing the human cerebral cortex on MRI scans into gyral based regions of interest. *Neuroimage* 31, 968–80. doi:10.1016/j.neuroimage.2006.01.021.

Glasser, M. F., Sotiropoulos, S. N., Wilson, J. A., Coalson, T. S., Fischl, B., Andersson, J. L., et al. (2013). The minimal preprocessing pipelines for the Human Connectome Project. *Neuroimage* 80, 105–24. doi:10.1016/j.neuroimage.2013.04.127.

Jack, C. R., Bernstein, M. A., Fox, N. C., Thompson, P., Alexander, G., Harvey, D., et al.

(2008). The Alzheimer's Disease Neuroimaging Initiative (ADNI): MRI methods. *J. Magn. Reson. Imaging* 27, 685–91. doi:10.1002/jmri.21049.

Kennis, M., van Rooij, S. J. H., Tromp, D. P. M., Fox, A. S., Rademaker, A. R., Kahn, R. S., et al. (2015). Treatment Outcome-Related White Matter Differences in Veterans with Posttraumatic Stress Disorder. *Neuropsychopharmacology* 40, 2434–42. doi:10.1038/npp.2015.94.

Mancini, M., de Reus, M. A., Serra, L., Bozzali, M., van den Heuvel, M. P., Cercignani, M., et al. (2016). Network attack simulations in Alzheimer's disease: The link between network tolerance and neurodegeneration. in *2016 IEEE 13th International Symposium on Biomedical Imaging (ISBI)* (IEEE), 237–240. doi:10.1109/ISBI.2016.7493253.

Marqués-Iturria, I., Scholtens, L. H., Garolera, M., Pueyo, R., García-García, I., González-Tartiere, P., et al. (2015). Affected connectivity organization of the reward system structure in obesity. *Neuroimage* 111, 100–106. doi:10.1016/j.neuroimage.2015.02.012.

Reess, T. J., Rus, O. G., Schmidt, R., de Reus, M. A., Zaudig, M., Wagner, G., et al. (2016). Connectomics-based structural network alterations in obsessive-compulsive disorder. *Transl. Psychiatry* 6, e882. doi:10.1038/tp.2016.163.

Repple, J., Meinert, S., Grotegerd, D., Kugel, H., Redlich, R., Dohm, K., et al. (2017). A voxel-based diffusion tensor imaging study in unipolar and bipolar depression. *Bipolar Disord.* 19, 23–31. doi:10.1111/bdi.12465.

Serra, L., Mancini, M., Cercignani, M., Di Domenico, C., Spanò, B., Giulietti, G., et al. (2016). Network-Based Substrate of Cognitive Reserve in Alzheimer's Disease. *J. Alzheimer's Dis.* 55, 421–430. doi:10.3233/JAD-160735.

Svatkova, A., Mandl, R. C. W., Scheewe, T. W., Cahn, W., Kahn, R. S., and Hulshoff Pol, H. E. (2015). Physical Exercise Keeps the Brain Connected: Biking Increases White Matter Integrity in Patients With Schizophrenia and Healthy Controls. *Schizophr. Bull.* 41, 869–

78. doi:10.1093/schbul/sbv033.

van Belle, J., van Hulst, B. M., and Durston, S. (2015). Developmental differences in intra-individual variability in children with ADHD and ASD. *J. Child Psychol. Psychiatry* 56, 1316–1326. doi:10.1111/jcpp.12417.

van der Burgh, H. K., Schmidt, R., Westeneng, H.-J., de Reus, M. A., van den Berg, L. H., and van den Heuvel, M. P. (2016). Deep learning predictions of survival based on MRI in amyotrophic lateral sclerosis. *NeuroImage Clin.* doi:10.1016/j.nicl.2016.10.008.

Van Essen, D. C., Ugurbil, K., Auerbach, E., Barch, D., Behrens, T. E. J., Bucholz, R., et al. (2012). The Human Connectome Project: a data acquisition perspective. *Neuroimage* 62, 2222–31. doi:10.1016/j.neuroimage.2012.02.018.

Verstraete, E., Veldink, J. H., Mandl, R. C. W., van den Berg, L. H., and van den Heuvel, M. P. (2011). Impaired Structural Motor Connectome in Amyotrophic Lateral Sclerosis. *PLoS One* 6, e24239+. doi:10.1371/journal.pone.0024239.

Walhout, R., Schmidt, R., Westeneng, H.-J., Verstraete, E., Seelen, M., van Rheenen, W., et al. (2015). Brain morphologic changes in asymptomatic C9orf72 repeat expansion carriers. *Neurology* 85, 1780–8. doi:10.1212/WNL.0000000000002135.

Yeh, F.-C., Wedeen, V. J., and Tseng, W.-Y. I. (2010). Generalized q-sampling imaging. *IEEE Trans. Med. Imaging* 29, 1626–35. doi:10.1109/TMI.2010.2045126.

Zalesky, A., Fornito, A., Harding, I. H., Cocchi, L., Yücel, M., Pantelis, C., et al. (2010). Whole-brain anatomical networks: Does the choice of nodes matter? *Neuroimage* 50, 970–983. doi:10.1016/J.NEUROIMAGE.2009.12.027.

Figure SI 1. Subnetworks identified by network based statistics. (A) Number of regions in the greatest component in thresholded version of the cross-disorder involvement map across a range of thresholds (0% - 100% cross-disorder involvement). The greatest components ranged from including all regions (at 0% cross-disorder involvement threshold) to including only one region (at 100% cross-disorder involvement threshold). At 35%, 40% and 45% cross-disorder involvement thresholds, the identified subnetwork showed significantly larger than subnetwork seen in subject-label permuted cross-disorder involvement maps (indicated by an asterisk *, $p < 0.05$). **(B)** Subnetworks and included regions (in blue) of the three identified significantly large subnetworks.

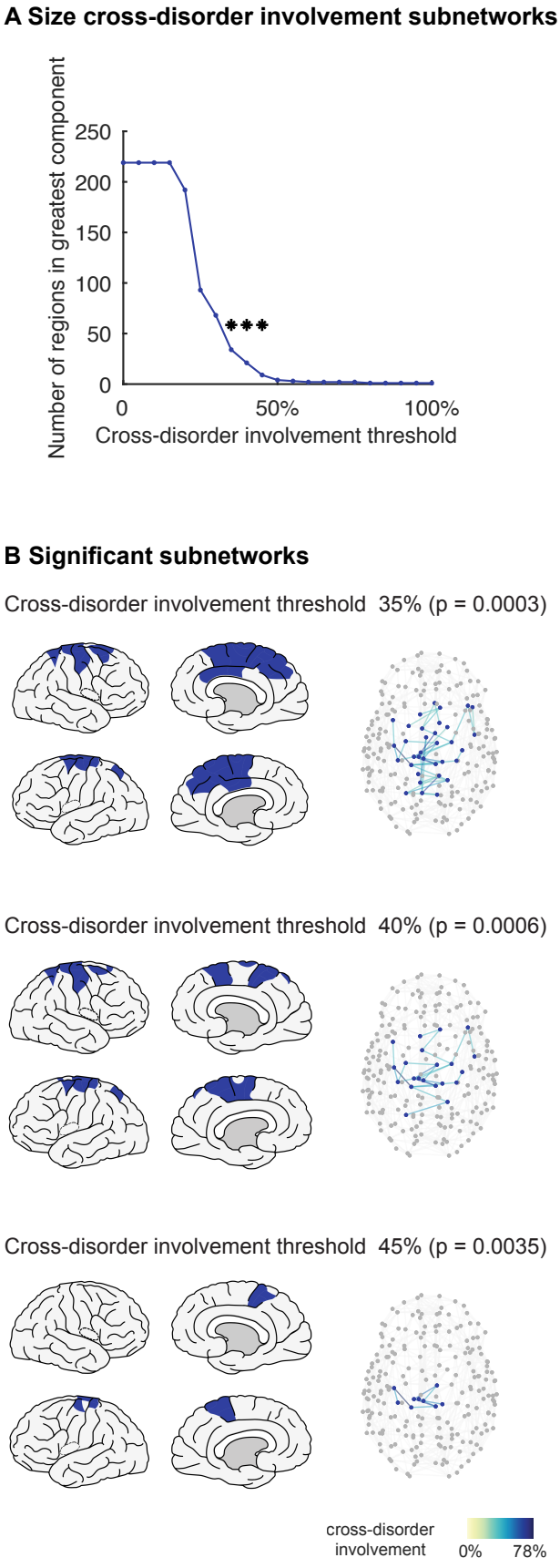

Figure SI 2. Rich club coefficient in reference connectome. Reference connectome data showed a significant rich club organization at all degree levels above 8 (indicated by an asterisk *, $p < 0.05$, FDR-corrected).

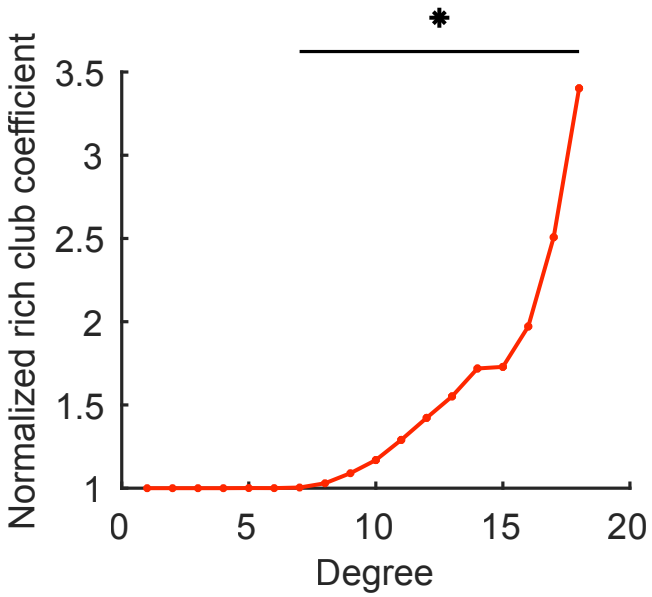

Figure SI 3. Rich club organization across percentages of hub regions. Ratio between cross-disorder involvement of rich club and local connections (left) and feeder connections (right). The ratios were evaluated for rich club, feeder and local connections derived from sets of hub regions selected at different percentages (7%, degree > 16; 9%, degree > 15; 13%, degree > 14; 18%, degree > 13; 25%, degree > 12). Percentages at which the ratio was significantly large (i.e. significant differences in cross-disorder involvement of rich club connections and feeder or local connections) are indicated by an asterisk * ($p < 0.05$).

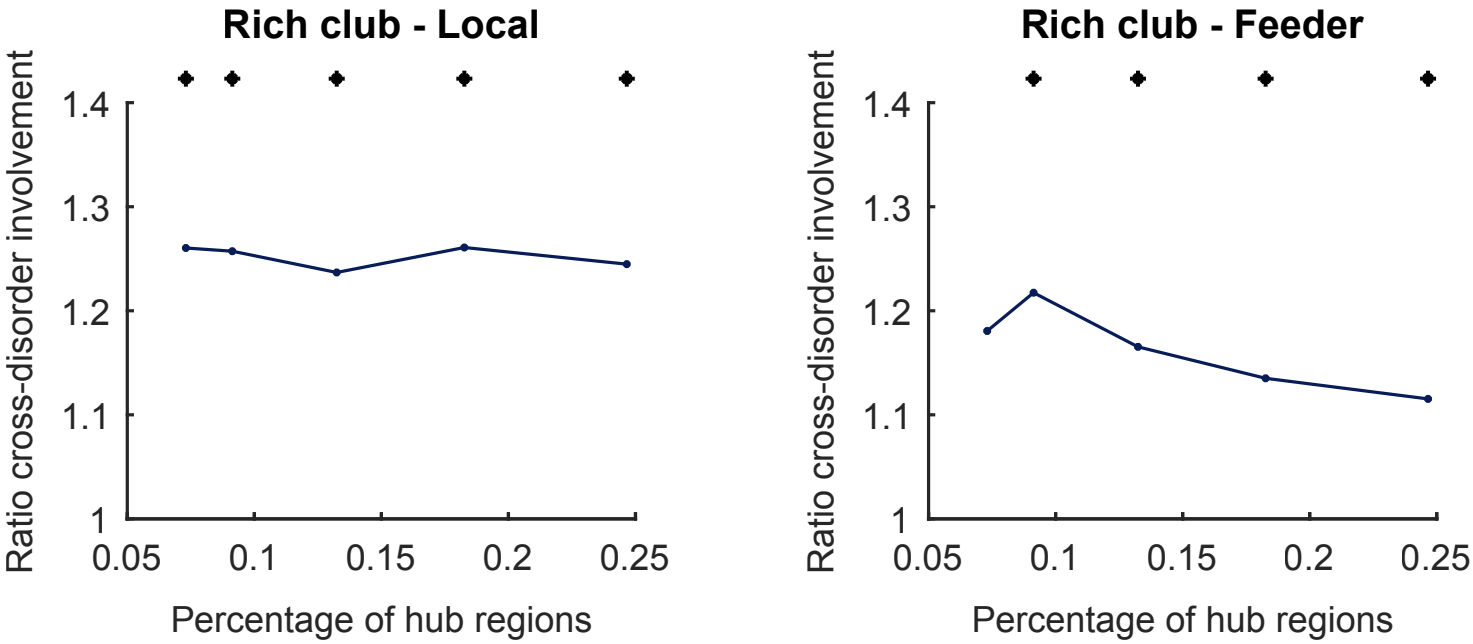

Figure SI 4. Edgewise network measures across percentages of central connections. The cross-disorder involvement of central connections (selected by edge betweenness (left), edge-removal effect on communicability (middle) and spatial wiring length (right)) relative to cross-disorder involvement observed in subject-label permuted cross-disorder involvement maps. The relative cross-disorder involvement was obtained at different selection percentages ranging from considering the top 5% most central connections to the top 45% most central connections. Percentages at which the ratio was significantly high (i.e. the set of central connections showed significantly higher cross-disorder involvement than in permuted cross-disorder involvement maps) are indicated by an asterisk * ($p < 0.05$).

A

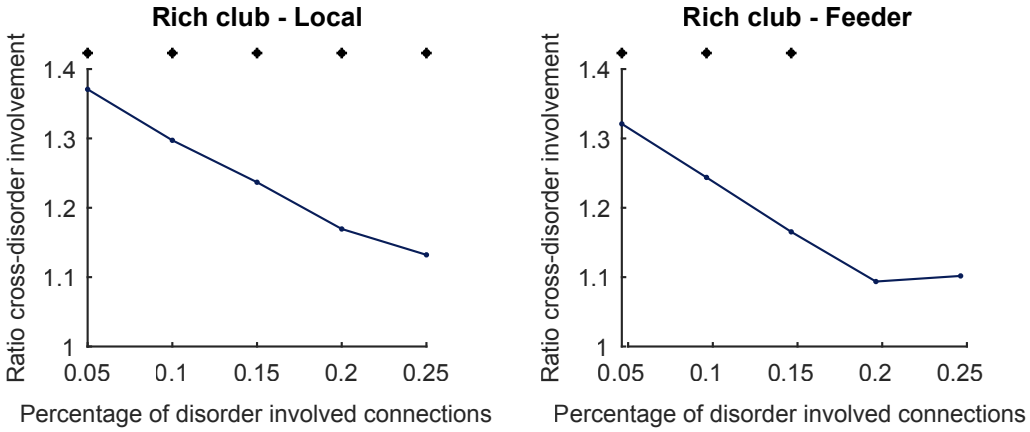

B

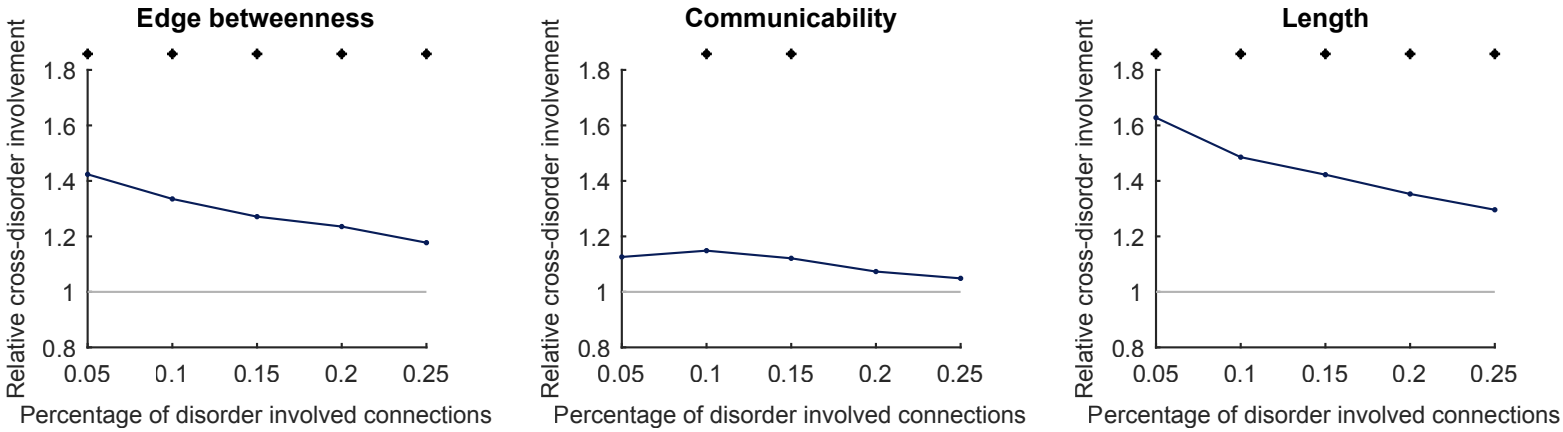

Figure SI 5. Cross-disorder involvement of central connections across percentages of disorder involved connections. Results were computed across various percentages of connections selected as disorder involved in addition to the 15% percentage used in the main analysis. **(A)** The ratio in cross-disorder involvement between rich club and local (left) and feeder (right) connections. **(B)** The relative cross-disorder involvement of central connections compared with subject-label permuted cross-disorder involvement maps. Significant effects are indicated by an asterisk * ($p < 0.05$).

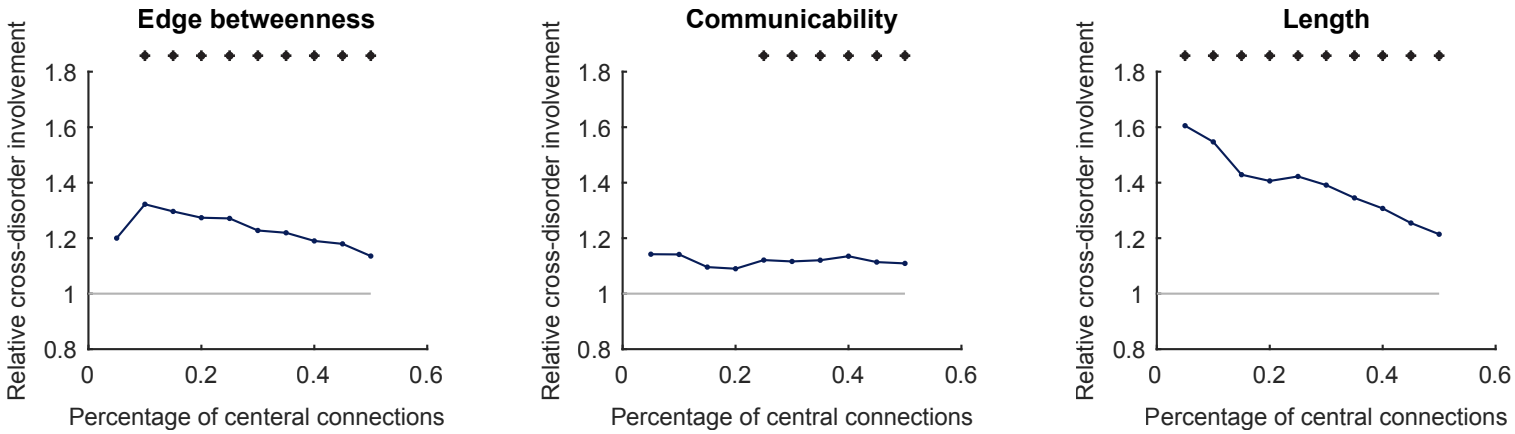

SI Table 1. Acquisition parameters of included datasets.

Disease	Voxel size T1 (mm×mm ×mm)	Voxel size DWI (mm×mm ×mm)	Protocol	B-weighting (s/mm^2)	Magnetic field strength	Reversed phase-encoding	References
ADHD	0.75×0.75×0.75	2×2×2	2×30	1000	3T	yes	[1]
ALS	0.75×0.75×0.75	2×2×2	2×30	1000	3T	yes	[2–4]
MCI I	1×1×1	2.3×2.3×2.3	1×61	1000	3T	no	[5]
MCI II	1.0×1.0×1.2	1.4×1.4×2.7	1×41	1000	3T	no	ADNI
OCD	1×1×1	2×2×2	1×32	1000	3T	no	[6]
PLS	0.75×0.75×0.75	2×2×2	2×30	1000	3T	yes	[2–4]
PTSD I	0.75×0.75×0.75	2×2×2	2×30	1000	3T	yes	[7]
PTSD II	1.0×1.0×1.2	1.4×1.4×2.7	1×41	1000	3T	no	DOD ADNI
Alzheimer's I	1×1×1	2.3×2.3×2.3	1×61	1000	3T	no	[5,8]
Alzheimer's II	1.0×1.0×1.2	1.4×1.4×2.7	1×41	1000	3T	no	ADNI
ASD	0.75×0.75×0.75	2×2×2	2×30	1000	3T	yes	[1]
Bipolar disorder	0.75×0.75×0.75	2×2×2	2×30	1000	3T	yes	[9]
MDD	0.5×0.5×0.5	0.94 ×0.94×3.6	1×20	1000	3T	no	[10]
Obesity	1×1×1	2×2×2	1×30	1000	3T	no	[11]
schizophrenia I	0.75×0.75×0.8	1.875×1.875×2	2×30	1000	3T	yes	[12]
schizophrenia II	0.75×0.75×0.8	1.875×1.875×2	2×30	1000	3T	yes	[13]

SI Table 2. Number of excluded subjects (because subjects miss information, subjects are considered outlier, or subjects are not matched) per dataset.

Cohort	Number of subjects	Number of subjects with missing information	Number of outliers	Number of not matched subjects	Number of subjects included in analyses
ADHD	49	0	2	0	47
ALS	427	0	9	328	90
MCI I	103	0	2	45	56
MCI II	115	0	3	0	112
OCD	83	0	6	0	77
PLS	78	0	3	11	64
PTSD I	73	0	3	0	70
PTSD II	92	0	5	7	80
Alzheimer's I	99	0	4	57	38
Alzheimer's II	56	0	3	0	53
ASD	49	0	0	0	49
Bipolar disorder	315	0	6	145	164
MDD	698	0	9	0	689
Obesity	63	0	1	0	62
schizophrenia I	225	0	4	7	214
schizophrenia II	107	18	3	40	46
total	**2681**	**18**	**62**	**640**	**1961**

SI Table 3. List of hub regions (region subnumbers are study specific).

left hemisphere - cuneus 1

left hemisphere - insula 2

left hemisphere – isthmus cingulate 1

left hemisphere - paracentral 2

left hemisphere – pars opercularis 2

left hemisphere – posterior cingulate 1

left hemisphere - precuneus 1

left hemisphere - precuneus 3

left hemisphere - precuneus 4

left hemisphere – superior frontal 1

left hemisphere – superior frontal 7

left hemisphere – superior frontal 8

right hemisphere – caudal anterior cingulate 1

right hemisphere – inferior parietal 6

right hemisphere - insula 2

right hemisphere - insula 3

right hemisphere – isthmus cingulate 1

right hemisphere – medial orbitofrontal 1

right hemisphere - postcentral 5

right hemisphere – posterior cingulate 1

right hemisphere – posterior cingulate 2

right hemisphere - precentral 6

right hemisphere - precuneus 3

right hemisphere - precuneus 4

right hemisphere - precuneus 5

right hemisphere – superior frontal 5

right hemisphere – superior parietal 7

right hemisphere – superior temporal 5

right hemisphere – temporal pole 1